Acoustic Properties of Porous Lead Zirconate Titanate Backing for Ultrasonic Transducers

Danjela Kuscer, Julien Bustillo, Tina Bakarič, Silvo Drnovšek, Marc Lethiecq, *Senior Member, IEEE*, and Franck Levassort, *Member, IEEE*

***Abstract*— For transducer design, it is essential to know the acoustic properties of the materials in their operating conditions. At frequencies over 15 MHz, standard methods are not well adapted because layers are very thin and backings have very high attenuation. In this article, we report on an original method for measuring the acoustic properties in the 15–25 MHz frequency range, corresponding to typical skin-imaging applications, using a backing/piezoelectric multilayer structure. Onto a porous $Pb(Zr_{0.53}Ti_{0.47})O_3$ (PZT) substrate, a piezoelectric PZT-based layer with a thickness of ∼20 μm was deposited and directly used to excite an acoustic signal into water. Herein, the measured signal corresponds to the wave that is first reflected on a target in water, then propagates back to the multilayer structure, and is transmitted through the thick film and further to the rear face of the porous backing, where it is again reflected and returns to the piezoelectric thick film, thus avoiding overlap with the electrical excitation signal. Two types of PZT backings with similar porosity of ∼20% and spherical pores with size of 1.5 and 10 μm were processed. The ultrasound group velocities were measured at ∼3500 m/s for both samples. The acoustic attenuation of the backings with pore size of 1.5 and 10 μm were 12 and 33 dB/mm, respectively, measured at 19 MHz. This advanced measuring technique demonstrated potential for the simple measurements of acoustic properties of backing at high frequencies in operating conditions. Importantly, this method also enables rapid determination of the minimum required thickness of the backing to act as a semi-infinite medium, for high-frequency transducer applications.**

***Index Terms*— Acoustic characterization, backing, porous $Pb(Zr_{0.53}Ti_{0.47})O_3$ (PZT).**

Manuscript received December 12, 2019; accepted March 21, 2020. Date of publication March 27, 2020; date of current version July 24, 2020. This work was supported in part by the Slovenian Research Agency under Grant P2-0105 and Grant L2-8180, in part by the Bilateral Project under Grant BI-FR-19-20-PROTEUS-08 and Grant 41658ZM, and in part by the ERASMUS Programme. The work of Danjela Kuscer was supported by Tours University through the GREMAN Laboratory. *(Corresponding author: Danjela Kuscer.)*

Danjela Kuscer and Silvo Drnovšek are with the Electronic Ceramics Department, Jožef Stefan Institute, SI-1000 Ljubljana, Slovenia (e-mail: danjela.kuscer@ijs.si; silvo.drnovsek@ijs.si).

Julien Bustillo and Marc Lethiecq are with the INSA Centre Val de Loire, GREMAN UMR7347 CNRS, 41000 Blois, France (e-mail: julien.bustillo@insa-cvl.fr; marc.lethiecq@insa-cvl.fr).

Franck Levassort is with Université de Tours, GREMAN UMR7347 CNRS, 37000 Tours, France (e-mail: franck.levassort@univ-tours.fr).

Tina Bakarič was with the Electronic Ceramics Department, Jožef Stefan Institute, SI-1000 Ljubljana, Slovenia, and also with the Jožef Stefan International Postgraduate School, SI-1000 Ljubljana, Slovenia. She is now with Krka, 8501 Novo mesto, Slovenia (e-mail: tina_bakaric@yahoo.com).

Digital Object Identifier 10.1109/TUFFC.2020.2983257

I. Introduction

POROUS piezoelectric ceramics have been largely studied as an active layer for ultrasonic transducer applications. The most commonly used piezoelectric material is based on lead zirconate titanate with a composition close to the morphotropic phase boundary that is $PbZr_{0.53}Ti_{0.47}O_3$ (PZT) [1].

The ultrasound transducer that operates at frequencies between 15 and 25 MHz consists of the piezoelectric layer with a thickness of a few tens of micrometers which is processed traditionally by machining a bulk piezoelectric ceramic or single crystal, or by thick-film technology [2]. According to the porosity content, several properties of the piezoelectric can be adjusted such as acoustic impedance, dielectric constant, and piezoelectric coupling factors [3]–[6]. Some properties of the porous ceramic can even be improved when compared with those of the dense ceramic with the same composition, in particular, the thickness coupling factor [7]. It was demonstrated that ∼30-μm-thick PZT with a relative density of 85%, a dielectric constant of ∼500, and a thickness coupling coefficient k_t of ∼0.4–0.5 can be processed on a porous ceramic substrate by screen printing or electrophoretic deposition, and consequent sintering at 800 °C–950 °C [8]–[11].

For transducer design, the active piezoelectric element is placed onto a backing, which allows acoustic energy to flow by the rear face. The closer is the acoustical impedance of the backing to that of the active layer, the more energy is lost. As a consequence, the corresponding transducer has lower sensitivity but higher axial resolution and bandwidth. Thus, a tradeoff between the sensitivity and the axial resolution/bandwidth has to be performed for each selected application. Moreover, the attenuation coefficient and the thickness of the backing must be sufficient so that no energy is radiated back to the active layer, which would produce parasitic echoes [1]. Porous ceramic can be used as backing since porous ceramic can satisfy all backing requirements, in particular, for frequencies over 15 MHz [8].

Our approach was to process a porous ceramic acting simultaneously as a highly attenuating backing and a mechanical support for subsequent deposition of bottom electrode and piezoelectric layer by the thick film technology. We refer to this sample as an integrated structure [8]. It should be noted here that ceramic backing possesses high mechanical stability at temperatures higher than 1000 °C, and thus supports the

high temperatures required for subsequent processing the electrode and the active piezoelectric layer, respectively. Since the backing has a similar chemical composition as that of the active piezoelectric layer, the diffusion processes and thermal expansion mismatch of the components are highly reduced during processing of the integrated structure. Also, the thick film technology avoids demanding and time-consuming thinning and gluing the piezoelectric bulk ceramic onto the backing, and is thus more efficient and more economic than the traditional process.

To properly design the transducer, the acoustic properties of the backing—acoustical impedance and attenuation—must be precisely known. Measurements were already performed at relatively low frequency of a few MHz, typically up to 5 MHz. Other ceramic compositions such as porous yttria-stabilized zirconia (YSZ) were also accurately characterized up to 4.5 MHz and results were compared with theoretical models [12], [13] for high-temperature transducer applications. The dependence of the attenuation with the pore size of the backing was clearly shown.

In previous work [9], we investigated Al_2O_3 and PZT ceramics with pore size below $\sim$10 μm for backing applications. Porous ceramic samples were processed by sacrificial template method that is based on the incorporation of a template into the ceramic powder. After the removal of the template, the pores are generated within the ceramic green body. By subsequent sintering, a ceramic with a porous microstructure was obtained [14]. The ceramic powder was mixed with template, ammonium oxalate, and then the powder compacts were heated to remove the template and sintered. The resulting ceramic had relatively homogeneous microstructure with a pore size of a few micrometers. The method is relatively simple; however, it restricts processing of ceramic with uniform predefined pore size and shape [9]. The characterization of the test single-element transducers which consisted of a 10-mm-thick porous ceramic backing, a metal bottom electrode, and $\sim$30-μm-thick PZT piezoelectric layer was performed in water. Electro-acoustic response with a center frequency around 40 MHz confirmed that the porous PZT and porous Al_2O_3 ceramics with a thickness of $\sim$10 mm are effective backings that can be considered as a semi-infinite medium. For many applications at high frequencies, miniaturization of the device is essential, which requires a reduction of the size of the backing since it is usually the largest constitutive element of the transducer. The backing should thus be as thin as possible which imposes a very high attenuation coefficient.

Ultrasonic spectroscopy has been used to measure acoustic properties of solid materials for ultrasonic transducers, such as phase and group velocities and attenuation coefficient. In particular, transmission [15] and reflection [16] methods in water have been extensively used for frequencies up to 10 MHz, but the data available at high frequencies are much more limited. These methods were nevertheless applied over 50 MHz for characterization of piezoelectric ceramics [17] and passive materials [18], but the partial cancellation of the reflected signal introduces some uncertainties in the measurement. An improved method [19] was proposed but it is also not appropriate for highly attenuating materials. Indeed, for such materials, the thickness of the sample must be quite small to have a sufficient quality of the transmitted signal. Specific methods have also been developed for thin polymer layers [20] or quarter wavelength acoustic matching layers [21].

In the present work, our objective is twofold. First, we propose a fabrication process of porous ceramic backings with pore sizes close to or smaller than the wavelength of the acoustic wave used for the characterization. For this, we use a sacrificial template method in combination with a hetero-coagulation (HC) process [22]. We assumed that with these procedures, we will process porous ceramics with a tailored amount of porosity, a tailored and uniform pore size, and a homogeneous distribution of the pores, and that the resulting ceramic will have a higher attenuation coefficient than those already reported in [9]. Polymethyl-metacrylate (PMMA) with spherical particles, available in different sizes, have been shown to be a useful template [14], [22]. In our previous work [23], we demonstrated that PMMA can be homogeneously distributed among PZT particles. After drying the suspension, pressing the powder mixture to a powder compact, subsequent debinding and sintering, we obtained ceramics with a homogeneous microstructure. The size, shape, and amount of pores in the ceramics were correlated with the amount, size, and shape of the added PMMA. Herein, median particle sizes of PMMA, 1.5 and 10 μm, were used for the fabrication of two types of backings, namely with pore size of $\sim$1 and $\sim$10 μm.

Second, for the high-frequency characterization of the backing, we will use integrated structures composed of porous PZT backings, a gold bottom electrode, a screen-printed piezoelectric PZT-based thick film with a thickness $\sim$20 μm, and a sputtered gold top electrode. These integrated structures with electrical connections can be considered as simple high-frequency transducers. Consequently, an original and straightforward way to measure acoustic properties of the backing directly at the operating frequency of the transducer was proposed. This method avoids the overlap of the electrical excitation and the measured signal, which regularly occurs with low-thickness backings. First, the electroacoustic responses of the two considered transducers immersed in water were measured. The characterization of the porous backing over 15 MHz was performed using the signal that was propagated to water, reflected on a target, returned toward the integrated structure, transmitted through the piezoelectric thick film and then to the rear face of the porous backing, and finally back to the active film. We then decreased the thickness of the porous backing and repeated the measurements. Properties such as group and phase velocities and acoustical attenuation in the bandwidth of the transducer were deduced in the frequency range 15–25 MHz. This method was also applied to another commercial porous material considered as a reference to verify the accuracy and the validity of deduced parameters. In addition, this *in situ* characterization allows to deduce the minimum thickness of the backing for miniaturized devices processed with mature ceramic technologies.

II. Experimental

A. Processing of the Porous Ceramic and Thick Films

Powders with the nominal composition $Pb(Zr_{0.53}Ti_{0.47})O_3$ (denoted PZT) and $Pb(Zr_{0.53}Ti_{0.47})_{0.98}Nb_{0.02}O_3$ with 2 mol% of excess PbO (denoted PZTNb) were synthesized by solid-state synthesis from PbO (99.9%, Aldrich), ZrO_2 (99.1%, Tosoh), TiO_2 (99.8%, Alfa Aesar), and Nb_2O_5 (99.9%, Sigma Aldrich). The oxides were homogenized in a planetary mill for 2 h. After drying, the mixtures were calcined at 900 °C for 1 h, remilled and recalcined at 1100 °C. After a second calcination, the powders were milled for 4 h and dried. Details are given in [24] and [25].

Spherical particles of PMMA with median particle sizes of 1.5 μm (PMMA1.5) and 10 μm (PMMA10) were used as templates (Soken Chemical and Engineering Co., Japan).

PZT suspension was prepared by stabilizing 10 vol% of PZT in water at pH 7 using 0.5 wt.% of polyethyleneimine (PEI, Alfa Aesar, Karlsruhe, Germany) with respect to the mass of the PZT. Separately, about 10 vol% of PMMA1.5 and PMMA10, respectively, were electrostatically stabilized in water at pH 7. The PZT and PMMA1.5 or PMMA10 suspensions, respectively, were mixed together in the volume ratio of 70:30. The suspensions were dried at 105 °C. Powder compacts with diameter of 12 mm and height of 10 mm were preheated at 400 °C for 1 h in the flow of a synthetic air and after that sintered at 1080 °C for 2 h in the PbO-rich atmosphere provided by the PZT packing powder. The description of the procedure is given in [23]. The ceramics obtained from the suspensions PZT mixed with PMMA1.5 and PZT mixed with PMMA10 are denoted as PZT1.5 and PZT10, respectively.

A gold electrode (ESL 8884-G) was screen-printed onto the top surface of the PZT1.5 and PZT10 cylinders and a gold contact was added on its lateral side. The gold paste was fired at 900 °C for 10 min with a heating rate of 30 °C/min.

A PZTNb paste was prepared from 60 wt.% PZTNb powder that was mixed with 40 wt.% of organic vehicle, comprising α-terpineol, ethylcellulose, and [2-(2-butoxi-etoxi-ethyl)] acetate. The PZTNb paste was screen-printed on the Au/PZT1.5 and Au/PZT10 cylinders, and the integrated structure was fired at 900 °C for 2 h. A top gold electrode was deposited on the piezoelectric PZTNb thick film using sputtering system 5 Pascal, Italy. The test samples prepared from PZT1.5 and PZT10 ceramics are denoted as T1.5 and T10, respectively.

The PZTNb thick films were poled at 150 °C for 15 min in an oil bath at 6 kV/mm and field-cooled to room temperature.

B. Characterization of the Suspensions, Ceramics, and Thick Films

The particle size distribution was determined using a static light-scattering particle size analyzer (Microtrac S3500, USA).

The zeta-potential (ZP) of the particles was measured using a ZetaPALS (Brookhaven, USA) ZP analyzer.

The phase composition of the samples was analyzed by X-ray powder diffraction (XRD) at room temperature using a PANalytical (X'Pert PRO MPD, The Netherlands) diffractometer. The data were collected in the 2Theta range from 20° to 70° in steps of 0.034°, with integration time of 200 s. The phases were identified using the software X-Pert High Score and the PDF-2 database [26].

The samples were mounted in an epoxy resin, ground and polished using standard metallographic techniques. The polished cross sections were analyzed by JSM 7600F scanning electron microscope (SEM; Jeol, Tokyo, Japan), equipped with an energy dispersive X-ray spectroscopy system (EDXS).

The relative density of the thick films was determined by quantification of the microstructure. The SEM images were turned into binary images using the image analysis software (ImageTools 3.0, University of Texas Health Science Center, San Antonio, TX) to quantify the volume fraction of pores [27]. Estimated accuracy of this evaluation is a few percent, which is equivalent or better than that of alternative methods such as mass and volume measurements or Hg-porosimetry, both of which could not be used directly on our samples. The relative densities of the thick films were calculated based on the theoretical density of $Pb(Zr_{0.52}Ti_{0.48})O_3$, which is 8.01 g/cm^3 (PDF 33–0784) [26].

The geometrical density ρ of the PZT1.5 and PZT10 ceramics was calculated from the mass and dimensions of the samples.

The dynamic sintering curves of the powder compacts were recorded upon heating with a heating rate of 5 K/min to 1200 °C in air using an optical dilatometer (Leitz V 1A, Leitz, Germany). The dimensions of the powder compacts were continuously measured from digitalized images and the relative shrinkage ($\Delta L/L$) was determined.

C. Electromechanical Characterization of Thick Films

The electromechanical properties of the piezoelectric thick films were deduced from the measurements in air of the complex electrical impedance around the fundamental thickness-mode resonance. The experimental set-up was composed of an HP4395A spectrum analyzer (Agilent Technologies Inc., Palo Alto, CA) and its impedance test kit.

The Krimholtz-Leedom-Matthaei (KLM) equivalent electrical circuit [28] was used to compute the theoretical behavior of the electrical impedance and a fitting process allowed the thickness mode parameters of the piezoelectric thick film to be deduced [8]. All the passive layers in the structure were taken into account that is gold bottom and top electrodes, and porous PZT backing. Parameters of these layers (velocity, density, and acoustical attenuation) were considered as constant values in the KLM model. For the thick film properties, five parameters were evaluated: the loss factors (mechanical, δ_m, and electrical, δ_e), the effective thickness coupling factor k_t, the longitudinal wave velocity c_L, and the dielectric constant at constant strain $\varepsilon_{33}^S/\varepsilon_0$.

D. Acoustic Characterization of Porous Ceramics

The two samples, T1.5 and T10, were inserted and glued with an epoxy resin in housing (polymer) with an external diameter (D_{ext}) of around 3 cm. This value is larger than the

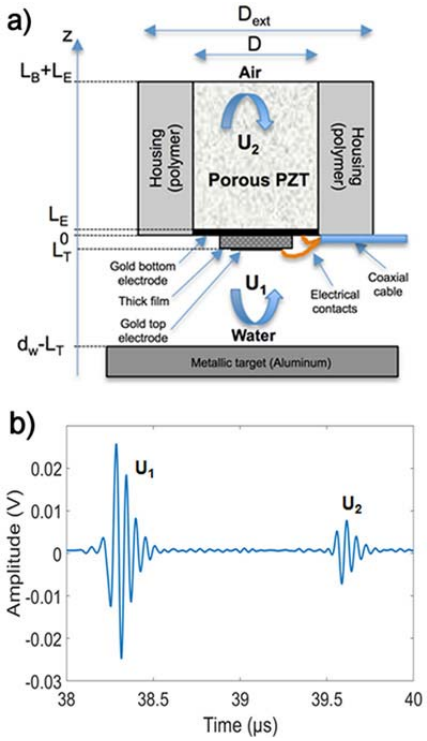

Fig. 1. (a) Schematic cross section of the structure used for acoustic characterization of porous PZT backing at high frequencies (L_T : thickness of the piezoelectric thick film, L_E : thickness of the bottom electrode, and L_B : thickness of the backing). (b) Measured signal U_1 (electroacoustic response of T1.5) in water from a distance d_w of 28.5 mm. Signal U_2 is measured for a thickness of the backing (L_B) of 2.1 mm.

diameter (D) of the porous PZT cylinder, ~10 mm. This configuration was chosen to facilitate the machining with silicon carbide sandpaper with a grit of 800 to reduce progressively step by step the thickness of the backing L_B (see Fig. 1) while keeping planar parallel surfaces of the cylinder. Electrical contacts were taken by two thin copper wires bonded to the electrodes. A coaxial cable (25 AWG, AlphaWire, Elizabeth, NJ, USA) with a characteristic impedance $Z_c = 50\ \Omega$ was used for the electrical connection to the generator.

For the acoustic characterization, the top faces of the two devices were immersed in water in front of a metallic target to first evaluate the electroacoustic response of the transducer. Rear faces of the backing stayed in air for all measurements. This allows the amplitude of the reflected wave to be maximized for the characterization. A pulser/receiver (PR5900, Panametrics,Waltham, MA, USA) was used with a 40 cm long 50-Ω cable (25 AWG, AlphaWire, Elizabeth, NJ, USA) to obtain the signal U_1 [see Fig. 1(a)] with a time of flight τ_{U1} on a digital oscilloscope corresponding to the electroacoustic response. This same wave partiallycontinues through the piezoelectric thick film, then bottom electrode toward the rear face of the backing, and finally back to the active film (signal U_2 which follows the signal U_1). If the porous backing is sufficiently thin, this signal can be observed as shown in Fig. 1(b). The time of flight of this U_2 signal (τ_{U2}) is sufficiently long to be completely separated from the initial electrical pulse excitation and U_1 signal. This is not the case of the signal directly emitted from the rear face of the piezoelectric layer which is superimposed with the electrical excitation [not shown on Fig. 1(b)]. The measurements are repeated several times, decreasing the thickness of the porous backing step by step by machining, from 3.5 mm to 500 μm. Properties such as group and phase velocities and acoustical attenuation in the bandwidth of the transducer can then be deduced.

The group velocity (c_G) in the backing with a thickness L_B is deduced from the measurements of times of flight τ_{U1} and τ_{U2} of the echoes U_1 and U_2, respectively, which are determined by an autocorrelation procedure

$$C_G = \frac{2L_B}{\tau_{U2} - \tau_{U1}} \tag{1}$$

This parameter is measured on each sample (PZT1.5 and PZT10) and is taken as reference value for the calculation of the backing acoustical impedance $Z_{0,B} = \rho \times c_G$, where ρ if the geometrical density.

It is often more convenient to use a frequency domain representation to obtain frequency-dependent parameters, such as phase velocity and acoustic attenuation. The signal U_1 can be expressed in frequency domain $U_1(f)$ as follows [16]:

$$U_1(f) = A_{\text{exc}}(f)e^{-2\alpha_w(f)d_w}e^{2jk_w(f)d_w}R_{w\text{-alu}}H_E(f)H_R(f) \tag{2}$$

with $A_{\text{exc}}(f)$ the spectrum of the excitation signal, $H_E(f)$ and $H_R(f)$ the transfer functions when the waves propagate in the medium in front of the emitter and receiver (in our case water), respectively, d_w the distance in water between the metallic target and thick film [see Fig. 1(a)], k_w the wavenumber in water, α_w the attenuation coefficient in water [10], and $R_{w\text{-alu}}$ the reflection coefficient (in amplitude) at the water/metallic target (aluminum) interface.

$U_1(f)$ is composed of several terms two of which correspond to the propagation inside the medium ($e^{2jk_w(f)d_w}$) and the attenuation term ($e^{-2\alpha_w(f)d_w}$). If the propagation medium is well known, such as water for our case, it is possible to determine them precisely. The reflection $R_{w\text{-alu}}$ can also be easily calculated using the acoustical impedances of water Z_w and aluminum Z_{alu} [29]. Moreover, assuming that the electrical excitation signal is short enough in time to consider its spectrum constant versus frequency, the transfer functions $H_E(f)$ and $H_R(f)$ can be estimated using the echo U_1

$$H_E(f)H_R(f) = \frac{U1(f)}{A_{\text{exc}}(f)e^{-2\alpha_w(f)d_w}e^{2jk_w(f)d_w}R_{w\text{-alu}}}. \tag{3}$$

In most cases, it can be assumed that the system is reciprocal, so the two transfer functions are considered as identical: $H_E(f) = H_R(f)$. Finally, the transfer function of the receiver $H_R(f)$ can be estimated

$$H_R(f) = \sqrt{\frac{U1(f)}{A_{\text{exc}(f)}e^{-2\alpha_w(f)d_w}e^{2jk_w(f)d_w}R_{w\text{-alu}}}}. \tag{4}$$

Fig. 2 shows this transfer function $H_R(f)$ calculated for the sample T1.5 using (4) and shows that the transducer has a center frequency at 19 MHz when the front medium is water.

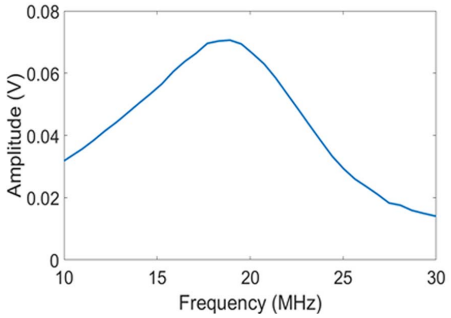

Fig. 2. Transfer function H_R of sample T1.5 as a function of frequency according to (4).

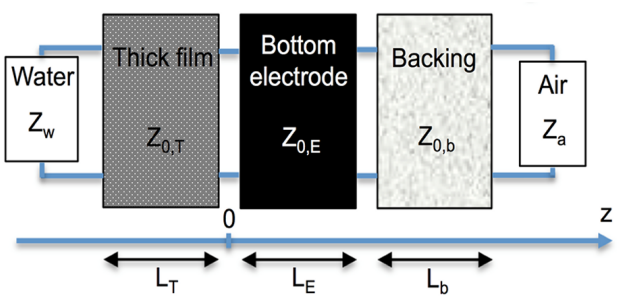

Fig. 3. Schematic representation of the two multilayer samples T1.5 and T10 for the transmission line theory.

TABLE I
PROPERTIES OF PZTNb PIEZOELECTRIC, GOLD ELECTRODE, AND PZT POROUS BACKING

Samples	Piezoelectric thick films		Gold bottom electrode		Backing (porous PZT)	
	t (μm)	ρ (kg/m^3)	t (μm)	ρ (kg/m^3)	ρ (kg/m^3)	PS (μm)
T1.5	22	6240	10	19300	6560	1
T10	22	6800	10	19300	6240	8

t: thickness; ρ: density; PS: pore size.

Using the same formalism, the echo $U_2(f)$ can be calculated using the propagation term inside the backing and the corresponding attenuation through it [15]

$$U_2(f) = U_1(f)e^{-2\alpha_B(f)L}e^{2jk_B(f)L}T_{B-T}(f) \times R_{B\text{-air}}(f)T_{T-B}(f)H_R(f) \quad (5)$$

with α_B the attenuation coefficient in the backing (porous PZT) and k_b the wavenumber in the backing. $T_{T-B}(f)$ and $T_{B-T}(f)$ are the transmission coefficients (in amplitude) between the thick film (T) and the backing (B), and inversely. $R_{B\text{-air}}(f)$ is the reflection coefficient (in amplitude) between the backing and air (rear face).

The thickness of the gold bottom electrode is not negligible when compared with that of the thick film as shown in Table I and this layer impacts the transmission of the ultrasonic wave in the structure. In $U_2(f)$ expression, this layer is taken into account in the transmission coefficients $T_{T-B}(f)$ and $T_{B-T}(f)$ through the transmission line formalism to calculate the acoustical impedances of the outgoing medium.

Fig. 3 gives the schematic representation of the samples T1.5 and T10 with the mechanical reciprocal of the electrical four-terminal model usually used in stepped transmission line theory, which was used for the calculation of the transmission coefficients $T_{T-B}(f)$ and $T_{B-T}(f)$ at $z = 0$. On contrary to the bottom electrode, the thickness of the gold top electrode of a few tens of nanometres can be neglected.

The terminal impedances are those of water (Z_w) in front of the transducer and air (Z_a) at the back. These two media are assumed to be semi-infinite. The input impedance Z_{i+1} at the interface between the media i and $i+1$ can be calculated using this equation

$$Z_{i+1} = Z_{0,i}\frac{Z_i + Z_{0,i}\tanh(k_iL_i)}{Z_{0,i} + Z_i\tanh(k_iL_i)} \quad (6)$$

where k_i is the wavenumber, L_i is the thickness, and $Z_{0,i}$ is the acoustical impedance of the considered medium i (i: T, E, or B for piezoelectric thick film, bottom electrode, and backing, respectively). The impedance Z_i corresponds to the input impedance in the medium i. Several intermediate calculation steps are used to deduce acoustical impedances $Z_B(f)$ and $Z_T(f)$ at $z = 0$.

Using these input impedances, the transmission coefficients T_{i-i+1} from the medium i to the medium $i+1$ are calculated using the standard following equation in the case of semi-infinite media:

$$T_{i-i+1} = \frac{2Z_{i+1}}{Z_{i+1} + Z_i}. \quad (7)$$

Finally, with (5), the attenuation coefficient $\alpha_B(f)$ and phase velocity $c_\varphi(f)$ in the backing are deduced [16]

$$\alpha_B(f) = \frac{-20\log_{10}\left(\left|\frac{U_2(f)}{U_1(f)T_{B-T}(f)T_{T-B}(f)R_{B\text{-air}}(f)H_R(f)}\right|\right)}{L_B} \quad (8)$$

$$c_\varphi(f) = \frac{4\pi f L_B}{arg\left(\frac{U_2(f)}{U_1(f)T_{B-T}(f)T_{T-B}(f)R_{B\text{-air}}(f)H_R(f)}\right)}. \quad (9)$$

E. Characterization of Gold Standard

To verify the accuracy of the procedure, we used commercial porous piezoelectric ceramic (Pz37, MEGGITT A/S, Kvistgaard, Denmark) for porous substrate [30] with porosity volume fraction of 83%. With this piezoelectric disk (diameter of 27 mm and a thickness of 2.9 mm), IEEE standard [31] was first used to deduce mechanical losses with the measurements of the electrical impedance around the fundamental resonance and the successive overtones (until the 19th corresponding to a frequency at 10.6 MHz) of the thickness mode. Beyond this value, the attenuation is too high for an accurate measurement. From this behavior of mechanical losses as a function of frequency, subsequent calculation was performed to deduce the attenuation coefficient α [32]. This procedure was also already applied to Pz37 [33] and compared with dense ceramic with similar composition. Second, gold bottom electrode and PZTNb thick film were successively screen-printed onto the

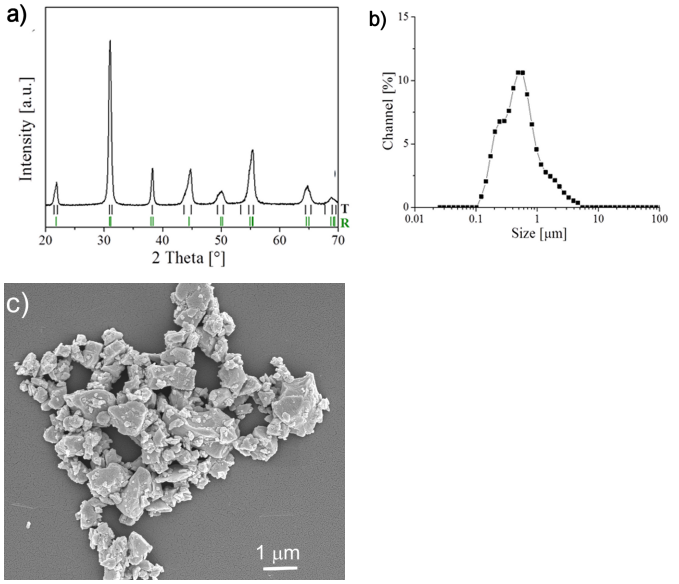

Fig. 4. $Pb(Zr_{0.53}Ti_{0.47})O_3$ (PZT) powder synthesized at 1100 °C. (a) XRD pattern. Calculated positions of hkl reflections are added for tetragonal (T; PDF: 33-0784), and rhombohedral (R; PDF:73-2022) phases. (b) Volume particle size distribution. (c) SEM micrograph.

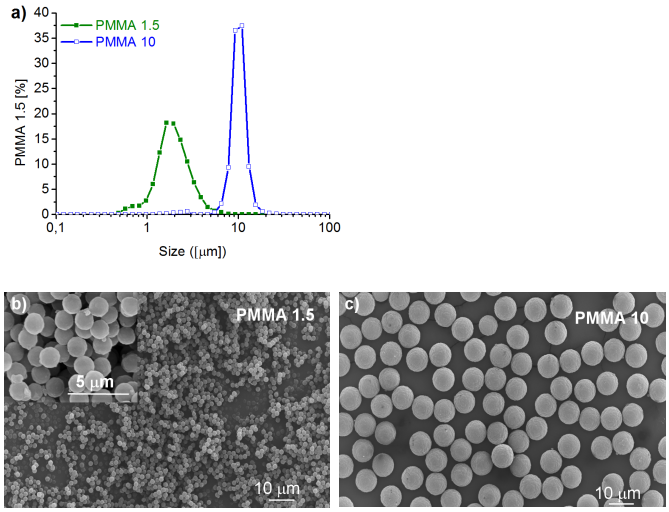

Fig. 5. (a) Particle size distribution of PMMA1.5 and PMMA10. (b) SEM micrograph of PMMA1.5. (c) SEM micrograph of PMMA10.

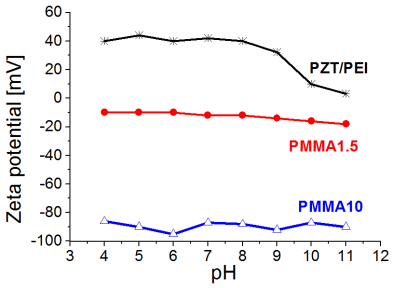

Fig. 6. ZP of PMMA1.5, PMMA10, and PZT stabilized with PEI as a function of pH.

top face on the same Pz37 disk and subsequently fired with the same procedure described in Section II-A. Top gold electrode was sputtered onto the thick film and poled at identical condition as KNNSr thick films in the samples T.1.5 and T10. The acoustic attenuation coefficient was measured in the same experimental condition as described in Section II-D for the samples T1.5 and T10.

III. Results and Discussion

A. Porous Ceramics With Tailored Size and Shape of the Pores

The porous ceramics were prepared from PZT powder synthesized at 1100 °C. The powder exhibited a perovskite crystal structure as a mixture of tetragonal (PDF 33-0784) and rhombohedral phase (PDF 73-2022) [see Fig. 4(a)]. The particle size ranged from ~0.1 to 4.6 μm with a d_{v50} of 0.4 μm, determined by laser granulometry [see Fig. 4(b)] which corresponded well to the SEM micrograph powder [see Fig. 4(c)].

Spherical polymetylmetacrylate particles with diameters of 1.5 (PMMA1.5) and 10 μm (PMM10) were used as templates. Both, PMMA1.5 and PMMA10 exhibited particles with narrow particle size distribution and a spherical shape with equal sizes of 1.5 and 10 μm, respectively (see Fig. 5).

We processed porous PZT ceramics using sacrificial template method from the suspension on the basis of the HC process of the oppositely charged PZT and template, PMMA particles in water followed by sintering. The HC was performed at room temperature. The key part of this process is to have the oppositely charged ceramic particles and organic template at the equal pH range to obtain homogeneous distribution of PZT and PMMA in the powder and subsequently in the ceramic. Thus, we investigated the ZP of the PZT and PMMA particles in water at room temperature as a function of pH. The ZP of the PMMA1.5 and PMMA10 particles in water was negative and did not vary significantly in the pH range between 4 and 11 (see Fig. 6). The ZP of PMMA1.5 was -90 ± 7 mV and the ZP of PMMA10 was -15 ± 5 mV. To obtain positive ZP of PZT particles in this pH range, PZT was stabilized in water with polyethyleneimine, PEI. The positive ZP of ~40 mV was measured between pH 4 and 8 as described elsewhere [34]. Based on ZP measurements, we selected a medium with pH 7 for processing the suspensions and for performing the HC process. In water at pH 7, the PZT particles stabilized with PEI had a positive ZP of $+42 \pm 5$ mV, while the PMMA1.5 and PMMA10 particles exhibited negative ZPs, i.e., -87 ± 5 and -12 ± 5 mV, respectively. At pH 7, the absolute values of the ZP are high enough and enable the effective dispersion of the particles in water, while the opposite charge on the PZT and PMMA particles should enable HC process.

Next, we prepared aqueous suspensions at pH 7 that is PZT stabilized with 0.5 wt.% of PEI, PMMA1.5, and PMMA10. The suspension of PZT particles and the suspension with PMMA particles were mixed together to obtain a PZT:PMMA powder mixture with a volume ratio of 70:30.

After the HC process and after drying the suspension, the PMMA1.5 were found to be homogeneously distrib-

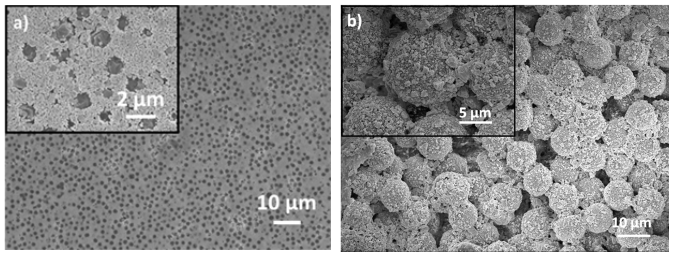

Fig. 7. SEM micrograph of the powder after HC. (a) PZT/PMMA1.5. (b) PZT/PMMA10.

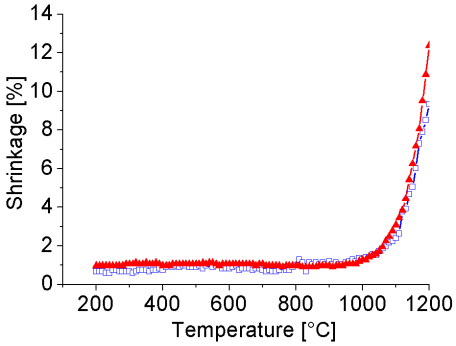

Fig. 8. Dynamic sintering curves for powder compacts prepared from PZT/PMMA1.5 (▲) and PZT/PMMA10 (□) powder mixture.

uted throughout the PZT powder [see Fig. 7(a)]. The larger PMMA10 particles were covered with the PZT particles forming a core-shell structure [see Fig. 7(b)]. It is evident that at pH 7, the PZT and PMMA particles exhibited opposite and high enough ZP which prevented the agglomeration of the equal particles and enabled the electrostatic attraction between PZT and PMMA particles causing the particles to flocculate together. Therefore, the HC process at pH 7 was efficient.

The sintering behavior of the powder mixture PZT/PMMA1.5 and PZT/PMMA10 was investigated using optical dilatometry. The results are shown in Fig. 8. Both powder compacts started to shrink at 940 °C. At 1000 °C, the sample showed a more pronounced densification (shrinkage) up to 1200 °C, where the shrinkage was ∼10% and ∼12% for PZT/PMMA10 and PZT/PMMA1.5, respectively. Based on the dynamic sintering curves of powder compacts, we selected 1080 °C as the sintering temperature for the processing of the porous ceramic.

Onto the PZT1.5 and PZT10 porous ceramic with a thickness of ∼3 and 3.5 mm, respectively, and diameter of ∼8 mm the gold electrode and PZTNb, respectively, were integrated using screen-printing and consequent sintering as described in Section II.

From the polished cross-section SEM micrographs of the samples T1.5 and T10 (see Fig. 9), it is evident that the piezoelectric PZTNb and gold electrodes of both the samples are similar. The PZTNb thick film was 22 μm thick with relatively homogeneous microstructure and a relative density of 78 ± 4 and 85 ± 4% for T1.5 and T10, respectively. The gold electrode was dense with a thickness of ∼10 μm. The piezoelectric film adhered well to the PZT porous ceramic and we have

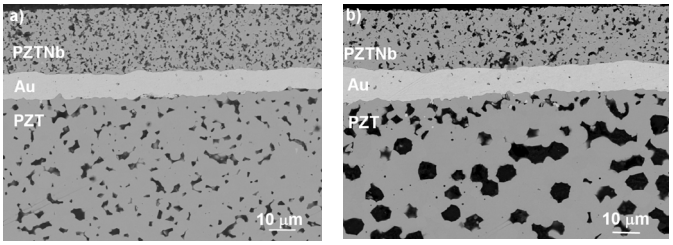

Fig. 9. Polished cross-section SEM image of the sample (a) T1.5 and (b) T10.

not observed any delamination. The microstructures of PZT porous ceramic were homogeneous with relative densities of 82% and 78% for T1.5 and T10, respectively, consistent with dynamic sintering curves [see Fig. 8]. The main difference between the two samples originates from different pore size of porous PZT. PZT in T1.5 contained micrometer-sized pores uniformly distributed in the PZT matrix having a grain size of 1.0 ± 0.4 μm, while PZT in T10 contained predominantly isolated spherical pores with a size of ∼8 μm in PZT matrix having a grain size of 3.2 ± 1.4 μm. It is evident that the size and the shape of the pores reflected the size and the shape of the PMMA templates as described in [23]. The results are summarized in Table I.

B. Electromechanical Properties of Thick Films and High Frequency Transducers

A fitting process of the electrical impedance of the integrated structures in air (before their integration in housing and electrical connection as shown in Fig. 1(a)) was used to deduce electromechanical properties of the piezoelectric PZTNb thick films. Several values from data in Table I were used as fixed parameters in the KLM model [8]: thickness and density of the thick films, density of the PZT porous backings, and thickness of the bottom electrode. Acoustic properties of gold were taken from [29]. Fig. 10 shows the electrical impedance of the transducer T1.5 in air (experiment and theoretical). Deduced properties of the PZTNb thick film in the sample T1.5 are given in Table II.

These properties are close to those obtained with a similar composition deposited by an EPD process [11]. Moreover, the effective thickness coupling factors are similar to that of standard bulk PZT, which ensures that sufficient sensitivity will be reached for backing characterization. For the T10 structure and gold standard, similar k_t was measured.

As shown on Fig. 10, the resonance frequency of the structure is around 30 MHz and the maximum value of the real part of the electrical impedance is low (<2.5 Ω). Moreover, the use of copper wires with small diameter for the electrical connections [see Fig. 1(a)] leads to a nonnegligible value of additional inductance. This led to the appearance of a cutoff frequency with the $R - L$ circuit which is at lower frequency than that of the structure, thus decreasing transducer performance [11]. In our case, with the experimental setup, the measured center frequency of the electroacoustic response decreased significantly and was at around 5 MHz [see Fig. 11(a)]. An alternative solution was to use a matching

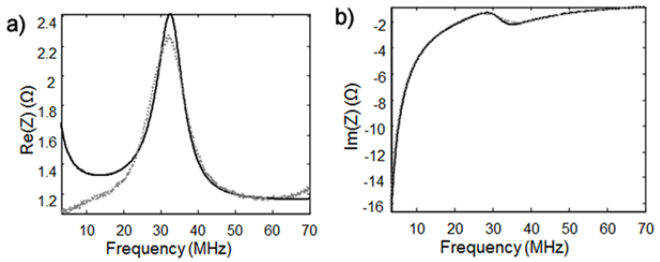

Fig. 10. Complex electrical impedance Z (a) real and (b) imaginary parts of PZTNb thick film multilayer structure of the sample T1.5 (solid black lines: theoretical and gray dashed lines: experimental values).

TABLE II
FUNCTIONAL PROPERTIES OF PZTNb THICK FILM IN SAMPLE T1.5

Sample	A (mm^2)	$\varepsilon_{33}^S/\varepsilon_0$	k_t (%)	δ_m (%)	δ_e (%)
T1.5	19.6	310	46	15	≈0.5

A: area of the top electrode; $\varepsilon_{33}^S/\varepsilon_0$: dielectric constant at constant strain; k_t: effective thickness coupling factor; δ_m: mechanical loss factor; δ_e: dielectric loss factor.

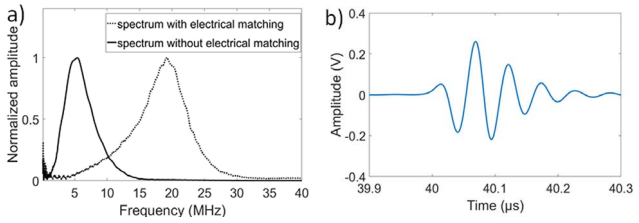

Fig. 11. (a) Frequency responses of T10 sample without (solid line) and with (dashed line) electrical matching. (b) Pulse-echo response of T10 sample (U_1 signal in water) with electrical matching.

electrical circuit, by adding a capacitance C between the copper wires and the piezoelectric structure to compensate the inductive effect of the copper wires with a *R-L-C* low-pass filter with a higher cutoff frequency. In our case, a capacitance of 100 pF was used to obtain a center frequency near 20 MHz [see Fig. 11(a)]. The corresponding pulse echo response of T10 sample is shown in Fig. 11(b). A tradeoff must be found between the additional noise and bandwidth. In our case, we do not choose to reach the resonant frequency of the multilayer structure without electrical connections (around 30 MHz, Fig. 10) to avoid a significant decrease of the sensitivity of the electroacoustic response. This electrical matching was used for the two structures and all following measurements.

The duration of this response [see Fig. 11(b)] at −6 dB is 400 ns and the corresponding fractional −6-dB bandwidth is around 40% (15–25 MHz).

C. Acoustic Characterization of Ceramics

For the structures T1.5 and T10, 3 and 13 measurements were successively performed by decreasing the thickness of the porous PZT backing from 3 to 1.3 mm and from 3.5 mm to 500 μm, respectively. For T10 sample with a thicknesses

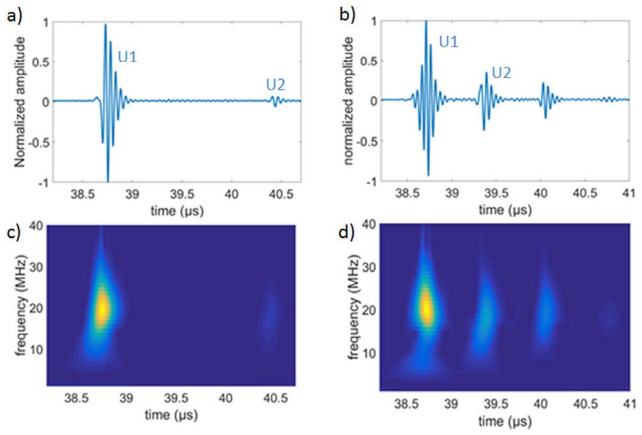

Fig. 12. Time responses (U_1 and U_2 signals) of T1.5 sample measured with a backing thickness of (a) 2930 μm and (b) 1150 μm and their respective wavelet transforms (c) and (d).

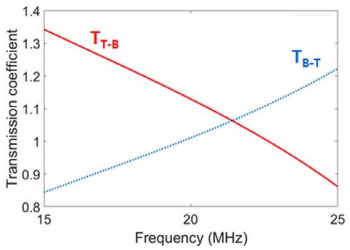

Fig. 13. Transmission coefficients (amplitude) T_{T-B} and T_{B-T} ($z = 0$, see Figs. 1 and 3) as a function of frequency for the sample T10.

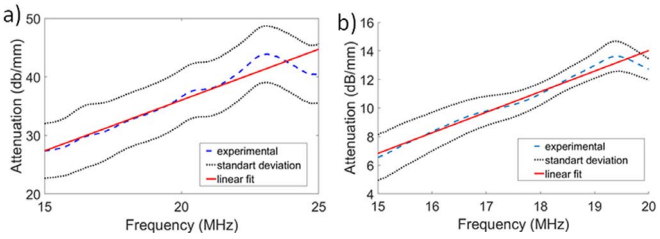

Fig. 14. Attenuation curves for (a) PZT1.5 and (b) PZT10. The experimental curves are in dashed lines and linear approximations in solid lines. Dotted lines correspond to the standard deviation.

of the backing higher than 2 mm, U_2 signal was not observed. Measurements only became possible under a certain value of the thickness for which signal U_2 came out of noise. For T1.5 sample, U_2 signal was measured even for the initial thickness of the backing, i.e., 3 mm, as shown on Fig. 12.

The group velocities are estimated at 3650 ± 30 m/s and 3400 ± 20 m/s for PZT1.5 and PZT10, respectively. These values are used to calculate the acoustical impedance $Z_{0,B}$, and the transmission coefficients T_{T-B} and T_{B-T} through the bottom electrode using (6) and (7). Fig. 13 shows the values and frequency dependence of these coefficients in the bandwidth of the transducer (for sample T10).

In the bandwidth of the transducer, i.e., ≈15–25 MHz, the phase velocity of PZT1.5 is between 3475 and 3515 m/s. The acoustic attenuations as a function of frequency are

represented in Fig. 14. As mentioned in Section III-B, several measurements were performed for different thicknesses of the backings. Herein, mean values with standard deviations are given. In a first approximation, linear behavior can be assumed to deduce the attenuation coefficient values: 1.7 dB/mm/MHz for PZT1.5 and 1.85 dB/mm/MHz for PZT10. At the center frequency of the transducers (19 MHz), measured attenuation is significantly higher in the PZT10 (around 33 dB/mm) than in the PZT1.5 (12 dB/mm). These values are coherent with those measured by Amini *et al.* [12] who found an attenuation around 2 dB/mm in the case of porous zirconia having 160-μm diameter spherical inclusions. It is noted that if the bottom electrode is neglected, attenuation is underestimated in both cases of around 3 dB and for the acoustic attenuation coefficient, calculated differences are less significant, with a decrease of around 0.15 dB/mm/MHz. The higher attenuation observed in PZT10 sample is consistent with the comparison between the pore sizes and the wavelength (around 170 μm at 19 MHz) where the scattering effects are usually reinforced [15] and consequently the acoustic attenuation. Moreover, Ciz *et al.* [34] have shown that the attenuation coefficient is similar for different pore radii but the overall attenuation is highly dependent on the pore radius random distribution. The backing processing method allows to have almost random distributions of the spherical pores and so the experimental results are in agreement with theory. Using these results, we can assume that the overall attenuation of porous PZT backings can be enhanced using higher pore diameters.

With the gold standard—porous Pz37 piezoelectric ceramic—we deduced the attenuation coefficient with the two methods. Using the measurement of the electrical impedance as a function of frequency, we obtain an attenuation coefficient of 0.57 dB/mm/MHz in the frequency range 5–10 MHz where a linear behavior is assumed as for the description on Fig. 14. With our procedure, we deduced in the same frequency range a value of 0.59 dB/mm/MHz. These results are identical to validate our new method.

IV. Conclusion

A method to characterize acoustic properties of PZT porous backing at high frequencies was described. The backings with tailored amount of porosity, homogeneous distribution of the pores having predefined size and shape were processed by a template method in combination with HC process and sintering. For measuring acoustic properties, piezoelectric integrated structures were used with two main advantages. First, the electroacoustic response of the structure itself is used to deduce group and phase velocities as well as acoustic attenuation coefficient. Second, this characterization is performed in the frequency range of interest (here 15–25 MHz) corresponding to the bandwidth of the transducer. Results for PZT porous backings with similar porosity of $\sim$20% but different pore diameters of $\sim$1 and $\sim$10 μm showed that group velocities are comparable (around 3500 m/s). The attenuation coefficients of the samples are comparable, 1.8 dB/mm/MHz. But, as expected, the acoustic attenuation depends on the pore sizes. The acoustic attenuation of the PZT10 sample at 19 MHz was 33 dB/mm, which is almost three times higher than that of PZT1.5, i.e., 12 dB/mm. Due to high acoustic attenuation coefficient of the PZT10 sample, the minimum thickness of the backing to consider it as a semi-infinite medium, is 2 mm. This low thickness value confirms that PZT porous ceramic with $\sim$10 μm sized pores is an interesting material applicable as a backing in miniature, high-frequency transducer applications. Our study was focused on the frequencies around 20 MHz but PZT10 would be even more efficient at higher frequencies where differences between wavelengths and pore sizes decrease. Consequently, the method developed here can not only be extended to higher frequencies, but also its use is even more justified as frequency increases because dimensions of elements become smaller and attenuation increases.

Acknowledgment

The authors would like to thank Mr. J.-Y. Tartu and Laurent Colin (Tours University) for assistance with the transducer fabrication.

References

[1] M. Lethiecq, F. Levassort, D. Certon, and L. P. Tran-Huu-Hue, "Piezoe lectric transducer design for medical diag sis and NDE," in *Piezoelectric and Acoustic Materials for Transducer Applications*, vol. 10, A. Safari and E. K. Akdoğan, Eds. Boston, MA, USA: Springer, 2008, pp. 191–215.

[2] M. Kosec, D. Kuscer, and J. Holc, "Processing of ferroelectric ceramic thick Films," in *Multifunctional Polycrystalline Ferroelectric Materials: Processing and Properties*, L. Pardo and J. Ricote, eds. Cham, Switzerland: Springer, 2011, pp. 39-61.

[3] H. Kara, R. Ramesh, R. Stevens, and C. R. Bowen, "Porous PZT ceramics for receiving transducers," *IEEE Trans. Ultrason., Ferroelectr., Freq. Control*, vol. 50, no. 3, pp. 289–296, Mar. 2003.

[4] A. N. Rybyanets, "Porous piezoceramics: Theory, technology, and properties," *IEEE Trans. Ultrason., Ferroelectr., Freq. Control*, vol. 58, no. 7, pp. 1492–1507, Jul. 2011.

[5] S. B. Lang and E. Ringgaard, "Measurements of the thermal, dielectric, piezoelectric, pyroelectric and elastic properties of porous PZT samples," *Appl. Phys. A, Solids Surf.*, vol. 107, no. 3, pp. 631–638, Jun. 2012.

[6] M. L. Dunn and M. Taya, "Electromechanical properties of porous piezoelectric ceramics," *J. Amer. Ceram. Soc.*, vol. 76, no. 7, pp. 1697–1706, Jul. 1993.

[7] F. Levassort, J. Holc, E. Ringgaard, T. Bove, M. Kosec, and M. Lethiecq, "Fabrication, modelling and use of porous ceramics for ultrasonic transducer applications," *J. Electroceram.*, vol. 19, no. 1, pp. 127–139, Oct. 2007.

[8] P. Maréchal, F. Levassort, J. Holc, L. P. Tran-Huu-Hue, M. Kosec, and M. Lethiecq, "High frequency transducers based on integrated piezoelectric thick films for medical imaging," *IEEE Trans. Ultrason., Ferroelectr., Freq. Control*, vol. 53, no. 8, pp. 1524-1533, Aug. 2006.

[9] P. Marechal *et al.*, "Electromechanical properties of piezoelectric integrated structures on porous substrates," *Ferroelectrics*, vol. 371, no. 1, pp. 89–97, Nov. 2008.

[10] D. Kuscer, F. Levassort, M. Lethiecq, A.-P. Abellard, and M. Kosec, "Lead-zirconate-titanate thick films by electrophoretic deposition for high-frequency ultrasound transducers," *J. Am. Ceram. Soc.*, vol. 95, no. 3, pp. 892–900, Mar. 2012.

[11] A.-P. Abellard, D. Kuscer, J.-M. Gregoire, M. Lethiecq, B. Malic, and F. Levassort, "Lead zirconate titanate-based thick films for high-frequency focused ultrasound transducers prepared by electrophoretic deposition," *IEEE Trans. Ultrason., Ferroelectr., Freq. Control*, vol. 61, no. 3, pp. 547–556, Mar. 2014.

[12] M. Amini, T. Coyle, and T. Sinclair, "Porous ceramics as backing element for high-temperature transducers," *IEEE Trans. Ultrason., Ferroelectr., Freq. Control*, vol. 62, no. 2, pp. 360–372, Feb. 2015.

[13] M. H. Amini, A. N. Sinclair, and T. W. Coyle, "A new high-temperature ultrasonic transducer for continuous inspection," *IEEE Trans. Ultrason., Ferroelectr., Freq. Control*, vol. 63, no. 3, pp. 448–455, Mar. 2016.

[14] A. R. Studart, U. T. Gonzenbach, E. Tervoort, and L. J. Gauckler, "Processing routes to macroporous ceramics: A review," *J. Amer. Ceram. Soc.*, vol. 89, no. 6, pp. 1771–1789, Jun. 2006.

[15] W. Sachse and Y. Pao, "On the determination of phase and group velocities of dispersive waves in solids," *J. Appl. Phys.*, vol. 49, no. 8, pp. 4320–4327, Aug. 1978.

[16] P. He and J. Zheng, "Acoustic dispersion and attenuation measurement using both transmitted and reflected pulses," *Ultrasonics*, vol. 39, no. 1, pp. 27–32, Jan. 2001.

[17] H. Wang, W. Jiang, and W. Cao, "Characterization of lead zirconate titanate piezoceramic using high frequency ultrasonic spectroscopy," *J. Appl. Phys.*, vol. 85, no. 12, pp. 8083–8091, Jun. 1999.

[18] H. Wang, T. Ritter, W. Cao, and K. K. Shung, "High frequency properties of passive materials for ultrasonic transducers," *IEEE Trans. Ultrason., Ferroelectr., Freq. Control*, vol. 48, no. 1, pp. 78–84, Jan. 2001.

[19] H. Wang and W. Cao, "Improved ultrasonic spectroscopy methods for characterization of dispersive materials," *IEEE Trans. Ultrason., Ferroelectr., Freq. Control*, vol. 48, no. 4, pp. 1060–1065, Jul. 2001.

[20] B. Hadimioglu and B. T. Khuri-Yakub, "Polymer films as acoustic matching layers," in *Proc. IEEE Symp. Ultrason.*, Dec. 1990, pp. 1337–1340.

[21] H. Wang, W. Cao, Q. Zhou, and K. K. Shung, "Characterization of ultra-thin quarter-wavelength matching layers of high frequency ultrasonic transducers," in *Proc. IEEE Symp. Ultrason.*, Oct. 2003, pp. 1048–1051.

[22] F. Tang, H. Fudouzi, T. Uchikoshi, and Y. Sakka, "Preparation of porous materials with controlled pore size and porosity," *J. Eur. Ceram. Soc.*, vol. 24, no. 2, pp. 341–344, Jan. 2004.

[23] T. Bakarič, T. Rojac, A.-P. Abellard, B. Malič, F. Levassort, and D. Kuscer, "Effect of pore size and porosity on piezoelectric and acoustic properties of $Pb(Zr_{0.53}Ti_{0.47})O_3$ceramics," *Adv. Appl. Ceram.*, vol. 115, no. 2, pp. 66–71, Feb. 2016.

[24] T. Bakarič, B. Budič, B. Malič, and D. Kuščer, "The influence of pH dependent ion leaching on the processing of lead-zirconate-titanate ceramics," *J. Eur. Ceram. Soc.*, vol. 35, no. 8, pp. 2295–2302, Aug. 2015.

[25] D. Kuscer, T. Bakarič, B. Kozlevčar, and M. Kosec, "Interactions between Lead–Zirconate titanate, polyacrylic acid, and polyvinyl butyral in ethanol and their influence on electrophoretic deposition behavior," *J. Phys. Chem. B*, vol. 117, no. 6, pp. 1651–1659, Feb. 2013.

[26] *International Centre for Diffraction Data. Powder Diffraction File. PDF-ICDD Version 2.2*, PCPDFWin, Newtown Square, PA, USA, 2002.

[27] M. Kuscer, M. Skalar, J. Holc, and M. Kosec, "Processing and properties of $0.65Pb(M_{g1/3}Nb_{2/3})O_30.35PbTiO_3$ thick films," *J. Eur. Ceram. Soc.*, vol. 29, no. 1, pp. 105–113, 2009.

[28] R. Krimholtz, D. A. Leedom, and G. L. Matthaei, "New equivalent circuits for elementary piezoelectric transducers," *Electron. Lett.*, vol. 6, no. 13, p. 398, 1970.

[29] A. R. Selfridge, "Approximate material properties in isotropic materials," *IEEE Trans. Sonics Ultrason.*, vol. 32, no. 3, pp. 381–394, May 1985.

[30] *Piezoelectric Ceramics*. Accessed: 2019. Nov. 12, [Online]. Available: https://www.meggittferroperm.com/wp-content/uploads/2017/10/Datasheet-Low-acoustic-pz37.pdf

[31] T. Meeker, "ANSI/IEEE standard On piezoelectricity," *IEEE Trans. Ultrason., Ferroelectr., Freq. Control*, vol. 43, no. 5, pp. 717–772, Jan. 1996.

[32] L. P. Tran-Huu-Hue, F. Levassort, N. Felix, D. Damjanovic, W. Wolny, and M. Lethiecq, "Comparison of several methods to characterise the high frequency behaviour of piezoelectric ceramics for transducer applications," *Ultrasonics*, vol. 38, nos. 1–8, pp. 219–223, Mar. 2000.

[33] M. Lethiecq *et al.*, "New low acoustic impedance piezoelectric material for broadband transducer applications," in *Proc. IEEE Ultrason. Symp.*, Aug. 2004, pp. 1153–1156.

[34] T. Bakarič, B. Malič, and D. Kuscer, "Lead-zirconate-titanate-based thick-film structures prepared by piezoelectric inkjet printing of aqueous suspensions," *J. Eur. Ceram. Soc.*, vol. 36, no. 16, pp. 4031–4037, Dec. 2016.

[35] R. Ciz, J. Toms, and B. Gurevich, "Attenuation and dispersion of elastic waves in a poroelastic medium with spherical inclusions," in *Proc. 3rd Biot Conf. Poromechanics*. Norman, Ok, USA: Univ. Oklahoma, 2005, pp. 201–207.

Danjela Kuscer received the Ph.D. degree from the University of Ljubljana, Ljubljana, Slovenia, in 1999. She is currently a Senior Researcher with Electronic Ceramics Department, Jožef Stefan Institute, Ljubljana, Slovenia, and an Associate Professor with Jožef Stefan International Postgraduate School, Ljubljana. Her research topics include synthesis of complex-composition ceramic materials, mainly piezoelectrics and ferroelectrics for electronic applications, formulation and characterization of suspensions, processing and patterning of thick film structures, and structural and microstructural characterization of materials. She is the author or coauthor of 130 publications, 150 technical reports, five patents, and one patent applications.

Dr. Kuscer was a member of the Organizing Committee of four international conferences. She is also a member of association MIDEM-Societey for Microelectronics, Electronic Components and Materials, Slovenian Chemical Society, and the International Society of Electrochemistry. She received the National Puh Recognition for achievements in research of ceramics in 2015 and awards Excellent in Science in 2016 in the field of technical science. She has been involved in about 20 projects. Since 2011, she has been an Associate Editor of the field technology and materials in journal *Informacije MIDEM*.

Julien Bustillo received the M.Sc. degree in microelectronics from the University of Dundee, Dundee, U.K., in 2011, the master's degree in engineering from the Ecole Nationale d'Ingénieur du Val de Loire, Blois, France, in 2011, and the Ph.D. degree in electronics from the University of Tours, Tours, France, in 2013.

He joined the GREMAN Laboratory, as an Associate Professor in 2014, where he is actually involved in the characterization of complex materials using ultrasound based methods. He is currently working on the characterization of porous materials involved in microelectronic applications as well as piezoelectric materials.

Tina Bakarič received the B.S. degree in chemistry from the University of Ljubljana, Ljubljana, Slovenia, in 2011, and the Ph.D. degree in nanosciences and nanotechnologies from Jožef Stefan International Postgraduate School, Ljubljana, in 2016.

From 2011 to 2016, she was a Young Researcher with Electronic Ceramics Department, Jozef Stefan Institute, Ljubljana. Since 2017, she has been an Independent Researcher with pharmaceutical company, Krka, Ljubljana. Her research interests include the preparation of ceramic suspensions, the fabrication of porous ceramics, and the fabrication of ceramic thick films by ink-jet printing.

Silvo Drnovšek graduated from the Faculty of Chemistry and Chemical Technology, Maribor, Slovenia, in 2002.

He is currently a researcher with Electronic Ceramics Department, Jožef Stefan Institute, Ljubljana, Slovenia. His research topics include preparation and characterization of powders using solid-state and mechanochemical synthesis, preparation and characterization of ceramics, thick films with screen printing technology, and multilayers by tape casting. He is the coauthor of about 270 publications and the coauthor of 13 patents or patent applications.

Dr. Drnovšek and his colleagues received Puh's recognition for achievements in research of alumosilicate ceramics in 2015.

Marc Lethiecq (Senior Member, IEEE) received the M.Eng. (Diplome d'Ingénieur) in electrical engineering and the M.Sc. (D.E.A.) degree in acoustics from the Institut National des Sciences Appliquées de Lyon (INSA Lyon), Villeurbanne, France, both in 1984, and the Ph.D. (Doctorat d'Ingénieur) degree in non-destructive testing from INSA Lyon in 1988.

From 1984 to 1987, he was a Teaching and Research Assistant at INSA Lyon. From 1987 to 1990, he had worked as a Research Engineer on ultrasonic transducers for biomedical and industrial applications at Vermon S.A. and CNTS. He was with the University of Tours, Tours, France, from 1990 to 2019. Since 1984, he has been teaching electronics, feedback control, applied physics, and courses related to his research activities in several universities and engineering schools. From 2012 to 2019, he was the Director of GREMAN, a joint research laboratory between University of Tours, CNRS, and INSA Centre Val de Loire on materials, microelectronics, acoustics, and nanotechnologies. He is currently a Professor at INSA Centre Val de Loire, Blois, France. He is also the Scientific Advisor for physics and nanoscience at the French Ministry in charge of Research and Innovation. His research is focused on ultrasonic transducers, piezoelectric materials and devices.

Franck Levassort (Member, IEEE) was born in near Paris, France. He received the bachelor's degree in applied physics and the D.E.A. (M.Sc.) degree in physical acoustics from University Paris 7-Denis Diderot, Paris, in 1990 and 1991, respectively, and the Ph.D. degree in ultrasound from the University of Tours, Tours, France, in 1996.

From 1997 to 2013, he was an Assistant Professor with the Institute of Technology, University of Tours, where he has been a Full Professor of electrical engineering since 2014 and he has been the Deputy Director of the GREMAN Laboratory since 2016. A Laboratory has more than 100 people in the field of materials, microelectronics, acoustics, and nanotechnology. His current research interests include design, modeling, characterization of piezoelectric materials and structures, and ultrasonic transducers for imaging applications.